Double-resonant Raman scattering in graphite: Interference effects, selection rules, and phonon dispersion

J. Maultzsch,[1] S. Reich,[2] and C. Thomsen[1]
[1]*Institut für Festkörperphysik, Technische Universität Berlin, Hardenbergstr. 36, 10623 Berlin, Germany*
[2]*Department of Engineering, University of Cambridge, Cambridge CB2 1PZ, United Kingdom*
(Received 9 February 2004; revised manuscript received 21 May 2004; published 8 October 2004)

We present a comprehensive analysis of double-resonant Raman scattering in graphite and derive an analytical expression for the Raman cross section of the *D* mode in one dimension. The extension to two dimensions does not change the double-resonant phonon wave vectors. In the full integration of the Raman cross section, the contributions by phonons from exactly the *K* point cancel due to destructive interference. We calculate the *D* mode explicitly based on recent experimental data of the graphite phonon dispersion. Applying the selection rules, a mapping of additional disorder-induced and second-order Raman modes onto the Brillouin zone of graphite is obtained.

DOI: 10.1103/PhysRevB.70.155403 PACS number(s): 78.30.−j, 63.20.Dj, 81.05.Uw

I. INTRODUCTION

Double-resonant Raman scattering reveals a variety of information about the electronic and vibrational states of a material. Double resonances, where two of the intermediate electronic states in the scattering process have to be real, usually require special experimental conditions. For example, an external electric field or pressure tune the electronic energies such that a double resonance occurs at a given excitation energy and with a zone-center phonon.[1,2] The double-resonance condition can be fulfilled more easily in a semimetal-like graphite,[3] but also in semiconductors with parabolic bands,[4] if the sample contains symmetry-breaking elements. Such defects are, e.g., the boundaries of the crystallites in polycrystalline graphite, or the crystal surface. They relax the quasi-momentum conservation and allow nonzero-phonon wave vectors to contribute to the Raman process. Alternatively, double resonances are observed in two-phonon Raman scattering, where momentum is conserved through phonons of equal but opposite wave vector. An example is the overtone spectrum of acoustic phonons in Ge.[5]

The characteristics of a double resonance is that the observed modes depend on the wavelength of the incoming light. At each excitation energy, a different phonon is selected by the double-resonance condition, resulting in the frequency shift of the double-resonant mode. Therefore, by changing the laser energy, one can measure the phonon dispersion, if the electronic band structure is known, or, vice versa, probe the electronic bands. In graphite, carbon nanotubes, and other forms of sp^2-bonded carbon, several defect-induced and second-order double-resonant modes are observed, of which the most prominent one is the so-called *D* mode at $\approx 1350\ \mathrm{cm}^{-1}$.

In this paper, we present a comprehensive treatment of defect-induced and second-order double-resonant Raman scattering in graphite based on the linear interpretation in Ref. 3. We discuss, in particular, the destructive interference of some of the scattering processes that are often mistakingly included in the literature. The difference between a two-dimensional and a one-dimensional integration is shown to be small. The recently experimentally determined phonon dispersion of graphite[6] and numerically derived electronic bands[7] allow us to explicitly calculate the *D*-mode line shape and its excitation-energy dependence without adjustable parameters. Both the absolute frequencies and the excitation-energy dependence of the *D* mode agree very well with the experimental Raman spectra. Furthermore, our results confirm that the *D*-mode phonons indeed stem from the transverse optical (TO)-derived branch, as predicted independently from symmetry and from a molecular approach.[8] We include the selection rules and use them to map the frequencies of other first- and second-order Raman modes onto the phonon dispersion of graphite.

The origin of the *D* mode in graphite and carbon nanotubes is well established as being defect-induced double-resonant scattering.[3,9,10] In spite of being intensively used, the double-resonance model is often incorrectly implemented or too severely simplified. In this introduction, we briefly explain the double-resonance process and then outline the issues that will be addressed in the following sections.

The defect-induced Raman process consists of four steps: Excitation of an electron–hole pair, inelastic scattering of the electron (or hole) by a phonon, elastic scattering of the electron (hole) by a defect, and recombination of the excited electron and hole. The second and third step can be interchanged; for the second-order Raman spectrum, the elastic defect scattering is replaced by inelastic scattering by a second phonon. The process is double resonant, if two of the transitions are real. By integrating the contributions of all allowed processes, irrespective of whether they are resonant or not, the Raman cross section can be computed. In Fig. 1, we show schematically the step of electron–phonon (electron-defect) scattering in the hexagonal Brillouin zone of the graphite sheet. The background is a contour plot of the conduction band. Scattering between two inequivalent *K* points, *K* and *K′*, leads to the *D* mode (solid arrows), whereas scattering close to the same *K* point or between two equivalent *K* points results in near-Γ point modes (dashed arrows).

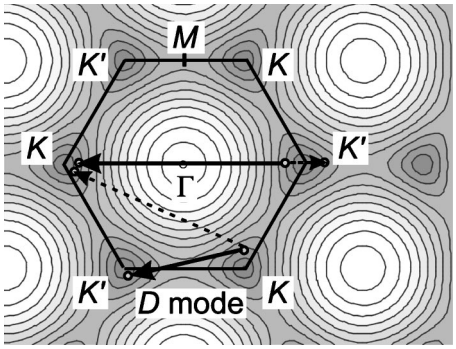

FIG. 1. Hexagonal Brillouin zone of graphene (single graphite sheet) with a contour plot of the conduction band (dark gray corresponds to zero energy). The high-symmetry points Γ, *K*, and *M* are indicated. Two neighboring *K* points, given by *K* and *K′*, are inequivalent, i.e., they cannot be transformed into each other by a reciprocal lattice vector. Their distance corresponds again to a *K*-point vector. Scattering between two inequivalent *K* points therefore results in the Raman *D* mode from near the *K* point (solid arrows). Scattering at the same *K* point or between two equivalent *K* points involves phonon wave vectors close to the Γ point (dashed arrows).

The double-resonance model provides an excellent understanding of all experimental observations of the *D* mode: The strength of the *D* mode increases with the number of defects in the sample;[11] it stems from near the *K* point of the graphite Brillouin zone. Its frequency depends on the wavelength of the exciting light and shifts at a rate of 38–70 cm^{-1}/eV.[12–16] Furthermore, the *D*-mode frequency is different in Stokes and anti-Stokes scattering, which can be understood from slightly different double-resonance conditions for the Stokes and the anti-Stokes process.[17] Many of the published applications of the double resonance, however, contain a number of conceptual problems when the Raman spectrum is calculated or the double resonance is used for a derivation of the phonon dispersion.

First, the full integration of the Raman cross section is often replaced by considering only the step shown in Fig. 1.[16,18–20] The wave vector $\boldsymbol{k}_i$ of the excited electron is fixed at the incoming resonance. Starting from this wave vector, the double-resonant phonon wave vectors $\boldsymbol{q}$ are determined, partly graphically[19] or by requiring that the electron wave vector $\boldsymbol{k}_b = \boldsymbol{k}_i - \boldsymbol{q}$ is real.[16,18–20] The calculation of the Raman spectra in this case is merely based on the condition that two intermediate electronic states have to be real. Although this is a necessary condition for double-resonant scattering, it is not sufficient for a large Raman signal. In such a simplified procedure, the Raman cross section may appear large for a particular phonon mode, but it vanishes in the complete integration by destructive interference. Neglecting the full integration therefore leads to incorrect predictions of the double-resonant Raman spectrum. Conversely, the phonon dispersion derived from double-resonant Raman scattering may be wrong, if interference effects are not taken into account. For example, the phonon from exactly the *K* point seems at first sight to contribute to the double resonance, but it is cancelled by destructive interference, as we will show in this paper. Nevertheless, the *K* point is often included in the derivation of the phonon dispersion, leading to incorrect results.[18,19] Thus, in the analysis of the *D* mode and other double-resonant modes, the interference effects have to be taken into account explicitly if the full integration of the Raman cross section is omitted.

Second, most of the full integrations have been carried out in one dimension only or for the one-dimensional case of carbon nanotubes.[9,16] Therefore, it needs to be clarified analytically how the two-dimensional integration in the graphite Brillouin zone affects the results obtained in one dimension.

Third, the symmetry and selection rules for electron–phonon scattering were frequently not considered. As a result, some double-resonant modes were assigned to a forbidden phonon branch, such as the assignment of the 800 cm^{-1} peak to the out-of-plane modes in Refs. 18 and 21. Even the *D* mode was incorrectly believed to belong to the longitudinal (LO)-derived phonon branch, which is degenerate at the *K* point.[3,9,16] Instead, it comes from the upper, fully symmetric phonon branch, which is nondegenerate at the *K* point.[8,15] We will confirm this explicitly by calculating the *D*-mode spectrum based on the newly obtained experimental phonon dispersion of graphite.

Finally, the quantitative analysis so far relied on—partly arbitrary—assumptions about the electron and phonon dispersion. The common tight-binding formula for the electronic band structure is a reasonable approximation if extended to including third-nearest neighbors.[7] In contrast, the phonon branches were often modeled by simple analytical expressions.[3,9,16] Because the theoretically determined phonon dispersions were contradictory in many respects, quantitative predictions of the *D* mode were difficult to judge. Here, we will use the experimental phonon dispersion of graphite for calculations of double-resonant *D*-mode scattering without any arbitrary assumptions.

This paper is organized as follows: In Sec. II, we give a detailed description of the integration of the Raman cross section, including interference effects and the integration in two dimensions. The selection rules for double-resonant scattering in graphite are derived in Sec. III. We calculate the *D*-mode spectra in Sec. IV and obtain a mapping of the additional double-resonant Raman peaks onto the phonon dispersion in Sec. V. In the Appendix, the derivation of the analytical expression for the Raman cross section is presented.

II. THEORY: INTEGRATION OF THE RAMAN CROSS SECTION

A. Double-resonant scattering in one dimension

In this section, we derive an analytical expression for the Raman cross section of the *D* mode in the approximation of linear bands in one dimension. The scattering process for the *D* mode takes place between two inequivalent *K* points of the graphite Brillouin zone, see Fig. 1. At the *K* point, the electronic bands are approximately linear for transition energies in the visible range of light and cross the Fermi level. Along the $\Gamma - K - M$ direction, the *D*-mode phonon wave vector is close to twice the *K*-point vector. In Fig. 2(a), both possibilities for scattering within the same electronic band are shown.

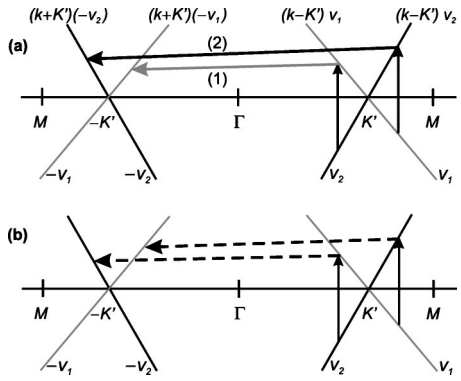

FIG. 2. (a) Double-resonant scattering processes leading to the *D* mode in graphite. The electronic bands are assumed to be linear at the *K* point with Fermi velocities v_1 and v_2. The *D*-mode scattering takes place across the Γ point within the same electronic band. (b) Scattering across the Γ point between two almost parallel bands does not contribute to the double-resonance signal because of destructive interference.

v_1 and v_2 are the Fermi velocities and k and q are the wave vectors of the electron and the phonon, respectively.

To find the double-resonant phonon wave vectors, the Raman cross section has to be evaluated by summing over all possible (including resonant and nonresonant) processes. The Raman cross section is proportional to $|K_{2f,10}|^2$, where the Raman matrix element $K_{2f,10}$ in higher-order scattering is given by[22]

$$K_{2f,10} = \sum_{a,b,c} \left[\frac{\mathcal{M}}{(E_1 - E_{ai})(E_2 - E_{bi})(E_2 - E_{ci})} + \frac{\mathcal{M}}{(E_1 - E_{ai})(E_1 - E_{bi})(E_2 - E_{ci})} \right]. \quad (1)$$

The matrix elements are assumed to be constant and are summarized by $\mathcal{M}$. E_1 and E_2 are energies of the incoming and scattered photons, respectively. The energy differences between the intermediate electronic states a,b,c and the initial state are denoted by E_{xi}. The first term in the sum corresponds to the process where the electron is first scattered by the phonon and then by the defect; in the second term of the sum this time order is reversed.

We first evaluate Eq. (1) for the two processes in Fig. 2(a). The evaluation of the sum is straightforward as shown in detail in the Appendix. Assuming $v_1 = -v_2$, we find from Eq. (1) for the scattering processes shown in Fig. 2(a)

$$K_{2f,10} = \frac{\mathcal{M}}{2v_1^2 \hbar \omega_{\mathrm{ph}}} \times \left[\frac{\kappa_1 + \kappa_2 + 2K' - q}{(\kappa_1 + K' - q/2)(\kappa_2 + K' - q/2)} \ln\left(\frac{\kappa_2 + K'}{\kappa_1 + K'} \cdot \frac{\kappa_1}{\kappa_2} \right) - \frac{\kappa_1 + \kappa_2 - 2K' + q}{(\kappa_1 - K' + q/2)(\kappa_2 - K' + q/2)} \ln\left(\frac{\kappa_2}{\kappa_1} \right) \right]. \quad (2)$$

Here, we defined κ_1 and κ_2 analogously to the approach in Ref. 3

$$\kappa_1 = \frac{E_1 - i\gamma}{2v_1} \quad \text{and} \quad \kappa_2 = \frac{E_1 - \hbar\omega_{\mathrm{ph}} - i\gamma}{2v_1}, \quad (3)$$

and K' denotes the wave vector of the K point. The lifetime broadening γ of the electronic transition energies is taken to be the same. Equation (2) depends on the phonon wave vector q and is evaluated as a function of q; the Raman intensity is at maximum for those q which fulfill the double-resonance condition. The maximum values of $K_{2f,10}$ are dominated by the terms in the denominators of Eq. (2). The double-resonant phonon wave vectors are, therefore,

$$q_{1,2} = 2(K' + \kappa_{1,2}) \quad \text{for} \quad k < K',$$

$$q_{3,4} = 2(K' - \kappa_{1,2}) \quad \text{for} \quad k > K', \quad (4)$$

where $q_{1,2}$ are double-resonant wave vectors with $q < 2K'$, i.e., they are between the K and M point and arise from process (1) in Fig. 2(a), whereas $q_{3,4}$ are between the Γ and K point [process (2) in Fig. 2(a)].

Compared to Eq. (2), the analytic expression derived by Thomsen and Reich[3] applies to scattering between different bands across the K point, as indicated by the dashed arrows in Fig. 1. Besides the change of the time order, there are two double-resonant phonon wave vectors only if the Fermi velocities are different. In contrast, Eq. (2) describes double-resonant scattering across the Γ point within the same band. Both processes, (1) and (2) in Fig. 2(a), are included, as well as both time orders of scattering by the phonon and by the defect. This leads to four different double-resonant phonon wave vectors [Eq. (4)], even if the Fermi velocities of both electronic bands are equal.

In the approximation of zero phonon energy, Eq. (4) for the double-resonant phonon wave vectors yields the so-called $q \approx 2k_i$ rule, where k_i is the wave vector of the incoming resonant transition. This approximation will be used below for mapping the double-resonant Raman modes onto the graphene Brillouin zone.

B. Interference effects

Interference effects are often neglected in the literature, when the full integration of the Raman cross section is omitted. They can, however, cancel some of the apparently double-resonant modes and thus significantly alter the Raman spectrum. An example is given in Fig. 2(b), where the electron is scattered across the Γ point between two different, almost parallel bands. In this process, at each excitation energy the double-resonance condition is fulfilled by the phonon exactly at the K point in the case of $v_1 = -v_2$. These phonons are often assumed to yield double-resonant terms with the phonon energy being independent of the excitation energy, see the data exactly at the K point in Refs. 18 and 19. When summing over all intermediate states these contributions, however, cancel, as we will show in this section. Moreover, in graphite the fully symmetric phonons leading to the *D* mode are not allowed to couple electronic states of different symmetry.

The Raman cross section for the scattering process shown in Fig. 2(b) can be evaluated in the same way as above, assuming $v_1 = -v_2$:

$$K_{2f,10}^{(b)} = \frac{2\mathcal{M}}{(2v_1)^3} \cdot \frac{f(q,\kappa_1,\kappa_2)}{(\kappa_1-\kappa_2)[2(\kappa_1-\kappa_2)+2K'-q]} \times \frac{1}{[2(\kappa_2-\kappa_1)+2K'-q](2K'-q)}, \quad (5)$$

where f is a function of q, κ_1, and κ_2 as defined in the Appendix. At first sight, this expression seems to have singularities at $q_1^{(b)}=2K'$ and $q_{2,3}^{(b)}=2K'\pm 2(\kappa_1-\kappa_2)$. In particular, $q_1^{(b)}=2K'$ agrees with what is found graphically from Fig. 2(b). The numerator [Eq. (A5)], however, vanishes simultaneously, and we obtain for $q\to 2K'$

$$\lim_{q\to 2K'} K_{2f,10}^{(b)} = \frac{2\mathcal{M}}{(2v_1)^3} \cdot \frac{1}{2(\kappa_1+K')(\kappa_2+K')}. \quad (6)$$

The Raman cross section is large if $\kappa_1=-K'$ or $\kappa_2=-K'$. For $\gamma=0$ this condition is equivalent to $E_{1,2}=-2v_1K'$, i.e., a laser energy that is resonant with the optical transition at $k=0$. Together with the initial condition of $q=2K'$ we conclude that such a scattering process is not reasonable and does not contribute to a double-resonance signal. The other possibilities result in a similar situation. From $q_{2,3}^{(b)}=2K'\pm 2(\kappa_1-\kappa_2)=2K'\pm\hbar\omega_{\rm ph}/v_1$ follows $\hbar\omega_{\rm ph}=\pm(qv_1-2K'v_1)$. This condition implies that either the phonon dispersion has the same slope as the electronic bands—in this case the process is "double-resonant" for any q—or, assuming a constant phonon energy, that $q\approx 2K'$. The latter case was already excluded above; the first is not realistic either. Therefore, we do not obtain double-resonant contributions from scattering across the Γ point between the two (almost) parallel electronic bands. Note that this mechanism is analogous to the destructive interference of double-resonant scattering within the same band, if the electron is not scattered across a minimum (or maximum) of the band. In fact, the destructive interference occurs because the electron before and after being scattered belongs to bands with the same slope, in particular with the same *sign* of the slope. Such contributions always vanish after the summation over all intermediate states, for details see also Ref. 22.

Interference effects do not only occur in the one-dimensional band structure discussed so far, but also in two or three dimensions, in particular, in the more realistic two-dimensional model system of graphene. In Fig. 3, we show the Raman intensity as a function of the phonon wave vector $|\boldsymbol{q}|$ obtained from a full calculation (solid line) and from the simplified procedure, where the electron wave vector $\boldsymbol{k}_i$ is fixed at the incoming resonance (dashed line). In the simplified calculation, the cross section is large for small $|\boldsymbol{q}|$ and diverges for $|\boldsymbol{q}|=0$. These contributions cancel in the summation over all initial electron wave vectors $\boldsymbol{k}_i$. The same effect occurs for the phonons exactly at the K point in graphite.

In summary, the contributions from $q=2K'$ [Fig. 2(b)] cancel as well as those from $q=0$. Nevertheless, when the integration of the Raman cross section is not performed explicitly but instead the double-resonant q vectors are found graphically, $q=0$ and $q=2K'$ contributions are often included by mistake.[16,18–20] Neglecting interference effects thus leads to incorrect results such as the prediction of Raman peaks

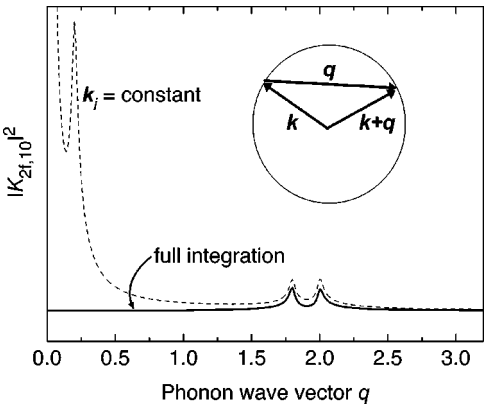

FIG. 3. Raman cross section as a function of the phonon wave vector calculated with a fixed incoming resonance (dashed line) and after the full integration (solid line). The large contributions at small q vanish by destructive interference in the integration. The solid line is the same as in Fig. 4, see Sec. II C for details. The inset shows the relation between the vectors $\boldsymbol{k}$ and $\boldsymbol{q}$ in Eq. (7).

that are not present in the spectra. In particular, $q=2K'$ corresponds to a K-point vector; this is included in the literature as a contribution fulfilling $|q-K|=0$ and being independent of the laser energy.[16,18–20] We showed, however, that it is not possible to obtain double-resonant Raman scattering with phonons from exactly the K point. The additional contributions that were incorrectly included led to wrong predictions about the phonon dispersion of graphite in the past.[18,19]

C. Double-resonant scattering in two dimensions

Finally, we discuss the differences between the one-dimensional integration above and an integration in two dimensions. Double-resonant scattering in two dimensions was mostly studied graphically, where entire circles of double-resonant phonon wave vectors were identified and used for an analysis of the experimental spectra. In this section, we show that again some of the graphically determined double-resonant q vectors vanish by destructive interference. Those wave vectors that correspond exactly to the one-dimensional integration are most enhanced in two dimensions as well. As an example we consider linear bands whch cross the Fermi level at $\boldsymbol{k}=0$ with a Fermi velocity v_1. Electrons are scattered across $\boldsymbol{k}=0$ from wave vector $\boldsymbol{k}$ to $\boldsymbol{k}+\boldsymbol{q}$, where $\boldsymbol{q}$ is the phonon wave vector, see inset to Fig. 3. In two dimensions, the cross section Eq. (1) can be written as an integral over $|\boldsymbol{k}|=k$ and the angle θ between the vectors $\boldsymbol{k}$ and $\boldsymbol{q}$

$$K_{2f,10}^{\rm 2D} = \frac{2\mathcal{M}}{(2v_1)^3}\int_0^\infty dk \int_0^{2\pi} d\theta \left[\frac{1}{(\kappa_1-k)(\kappa_2-k)} \times \frac{1}{\kappa_{1,2}-(k+\sqrt{k^2+q^2+2kq\,\cos\,\theta})/2} \right], \quad (7)$$

with κ_1 and κ_2 as defined in Eq. (3). $|K_{2f,10}^{\rm 2D}|^2$ is plotted as a function of $|\boldsymbol{q}|$ in Fig. 4 for $\kappa_1=1-0.01i$ and $\kappa_2=0.9-0.01i$ (upper curve). The lower curve is the same scattering process evaluated in one dimension. The positions of the maxima, i.e., the phonon wave vectors that contribute most in the

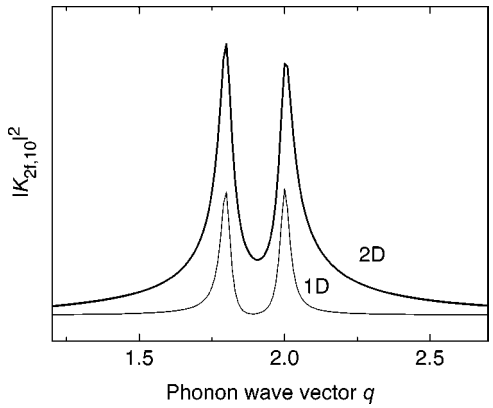

FIG. 4. Raman cross section $|K_{2D}|^2$ as a function of the phonon wave vector for linear bands in one dimension (lower curve) and for linear bands in two dimensions (upper curve).

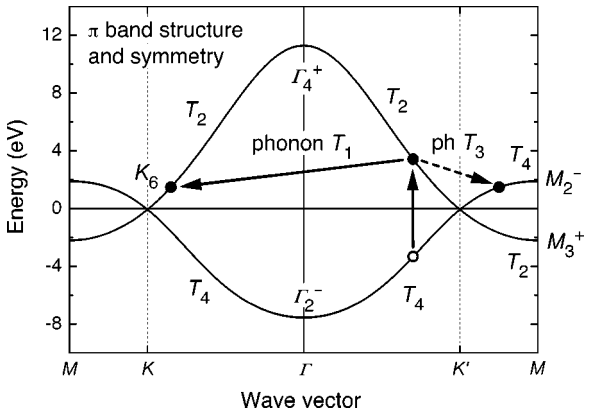

FIG. 5. Electronic π and π^* bands of graphene along $\Gamma-K-M$. The symmetry of the bands is given. The solid arrows denote the same double-resonant process as in Fig. 2(a). Only fully symmetric (T_1) phonons can contributeto the scattering within the same nondegenerate band. The dashed arrow indicates another possibility of double-resonant scattering, involving phonons from near the Γ point with T_3 symmetry.

double-resonance, are the same in both calculations. The main difference is the broader range of double-resonant q vectors, if the integration is performed in two dimensions.

Several authors estimated the relative weight of the contributions to the double-resonance signal by considering a "density" of double-resonant phonon wave vectors in two dimensions.[19,20] Our results show that the main contributions come from scattering across the Γ or K point as in one dimension. Therefore, to find the double-resonant phonon wave vectors with the strongest Raman signal, the integration in one dimension is sufficient.

III. SELECTION RULES

In the preceding section, the possible double-resonant Raman processes in graphite were analyzed from a purely mathematical point of view. Each phonon branch yields double resonances in the framework of the discussion presented so far. It has been argued that double-resonant Raman scattering cannot explain the selective enhancement of the D band with respect to other phonon branches in graphite.[15,23] In this section, we include the symmetry of electrons and phonons and analyze which of the phonon branches are allowed by selection rules in double-resonant scattering. Based on this analysis the TO branch of graphite is expected to yield the largest Raman cross section, whereas the out-of-plane modes are never double resonant.

Figure 5 shows the electronic π and π^* bands in graphene along $\Gamma-K-M$; they are labeled by their symmetry. The bands are calculated from the tight-binding approximation including third-nearest neighbors and fit to ab initio results.[7] Along $\Gamma-K-M$, the wave vectors between the high-symmetry points belong to the C_{2v} subgroup of the D_{6h} point group of graphene. The electronic bands have either T_2 or T_4 symmetry (A_2 and B_2 in molecular notation). The double-resonant process (1) from Fig. 2(a) is shown by solid arrows. The optical transition between T_4 and T_2 requires a photon with Γ_6^- symmetry, i.e., in-plane polarized light. The excited electron is then scattered within the same band by a phonon. The phonon must therefore be fully symmetric (T_1). The same selection rules hold for the second process in Fig. 2(a), because the electron–phonon scattering again takes place within the same electronic band.

We assume that the defect-scattering does not change the symmetry of the electron. Even if it changed the symmetry, the Raman cross section would be small, because the defect had to couple electronic states of different symmetry. In the example shown in Fig. 5, the third intermediate electronic state is in this case far away from a real electronic state with the correct symmetry. Therefore, the third term in the denominator of the Raman cross section [Eq. (1)] is much larger than for an intermediate state very close to a real state.

The double-resonant phonon wave vectors are, as shown in the previous section, near $q=2K'$, which corresponds to near-K point vectors. At the K point of graphene, there are two optical branches, one derived from the LO and one from the TO Γ-point phonon. Although the eigenvectors at the K point are of mixed longitudinal and transverse character, we call them TO and LO for convenience. At the K point, the TO is the upper branch, which is fully symmetric (K_1 or A_1') in the D_{3h} symmetry group of the K point; the LO (lower branch) is degenerate with the longitudinal acoustic mode (K_5 or E' symmetry). Between the high-symmetry points the TO and the LA phonons have T_1 symmetry; the LO and the in-plane TA phonons belong to the T_3 representation. The out-of-plane modes have T_2 and T_4 symmetry. Therefore, not all phonon branches contribute to the double resonance process as expected when neglecting symmetry. Only phonons from the TO or the LA branch are allowed in the double-resonant scattering shown in Fig. 2(a). Because the LA does not have the correct symmetry at the K point nor at the Γ point, we expect from continuity that the TO branch, which is allowed at both K and Γ, leads to the strongest double-resonant Raman signal. The LO phonon is forbidden by symmetry in the D-mode process, in contrast to a variety of models which regarded the LO responsible for the Raman D mode.[3,13,18,24] The reason for the LO being involved in those calculations is that most theoretical predictions[25–27] of the LO branch provided the characteristics required to match the

experimental data of the *D* mode. These requirements are a frequency at about 1250 cm^{-1} and a local minimum at the *K* point. The TO phonon was predicted at a too high frequency at the *K* point, e.g., 1370 cm^{-1} in the ab initio calculation of Ref. 27. In force-constants calculations even a local maximum was found for the TO branch at the *K* point,[25] which is incompatible with the positive frequency shift as a function of laser energy. On the other hand, a fully symmetric breathinglike vibration of the carbon hexagons was suggested already by Tuinstra and Koenig[11] and later predicted from a molecular approach based on small aromatic molecules.[8,15,23,28] Only recently the correct TO and LO branches of graphite were found from inelastic X-ray scattering.[6] In the following section, we show that when using this new experimentally determined phonon dispersion, indeed the calculations from the TO phonons match the experimental *D*-mode spectra very well.

So far we considered scattering of the electrons across the Γ point within the same band. The electron can also be scattered across the *K* point, i.e., between different bands, leading to further defect-induced modes with wave vectors closer to the Γ point. This is shown in Fig. 5 by the dashed arrow. The symmetry of the phonon required for scattering between electronic states with T_2 and T_4 symmetry is T_3, therefore in this process the LO and TA modes are allowed. The contribution from the defect scattering step, however, will be rather small because either the third intermediate state is not close to a real state of the same symmetry (if the defect conserves symmetry) or the scattering probability is small (if the defect changes symmetry). Therefore, defect-induced modes from close to the Γ point are predicted to be weaker than the *D* mode.

For *D*-mode scattering in carbon nanotubes,[9] there is a symmetry-based objection against the LO phonon as well. In armchair tubes, the LO-derived phonon branch has odd parity with respect to the vertical mirror plane.[29] The incoming and outgoing light in the Raman process (*zz*-polarization) has even parity and, hence, does not change the parity quantum number of the system. Therefore, the odd-parity LO phonon is in fact forbidden. In chiral tubes, however, these parity quantum numbers do not exist and both phonon branches are allowed.

IV. CALCULATION OF THE *D* MODE

We now use the analytical expression derived for the Raman cross section, Eq. (2), to calculate the *D* mode of graphite. The average slope of both electron bands at the *K* point was set to $v_1 = -5.1$ eV Å from a fit to ab initio calculations of the electronic band structure for transition energies below 3 eV.[7] For the phonons, we used a linear fit of the experimental TO frequencies close to the *K* point.

Figure 6 shows the *D*-mode frequencies calculated from the TO branch (solid lines) together with the experimental values for graphite. The *D* mode consists of two groups of peaks, one from each side of the *K* point [process (1) and(2) in Fig. 2(a)]. These two groups correspond to $q_{1,2}$ and $q_{3,4}$ from Eq. (4), respectively, see inset to Fig. 6. Within each group, a double-peak structure results from the two different

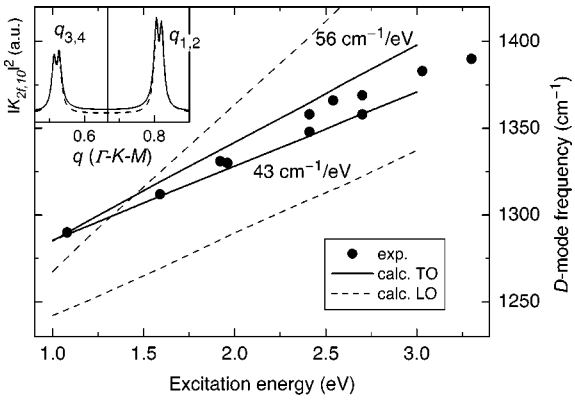

FIG. 6. *D*-mode frequency of graphite as a function of laser energy. The dots denote experimental data from Refs. 13, 30, and 31. The lines are calculations for defect-induced Raman scattering based on the experimental data for the TO (solid line) and LO (dashed line) phonon branch around the *K* point. Inset: Raman intensity $|K_{2f,10}|^2$ as a function of the phonon wave vector q at $E_1 = 2.0$ eV. The solid line is from a calculation of Eq. (2); for the dashed line the scattering process in Fig. 2(b), i.e., scattering by *K*-point phonons, was explicitly included. These phonons (vertical line) do not contribute to the Raman signal due to destructive interferences. $q_{1,2}$ and $q_{3,4}$ correspond to Eq. (4).

time orders in the scattering process. In Fig. 6, the average of the peak positions in each group was taken. The calculated slopes are 56 cm^{-1}/eV and 43 cm^{-1}/eV, where the larger slope stems from phonon wave vectors between *K* and *M* and the smaller one between *K* and Γ. Compared to the experimental slopes of 44 cm^{-1}/eV (Ref. 13), 47 cm^{-1}/eV (Ref. 30), and 51 cm^{-1}/eV (Ref. 31), we find a very good agreement. In contrast, if we calculate the *D* mode from the LO data (dashed lines), either the Raman frequencies are by 40–50 cm^{-1} lower than the experimental values, or the *D* mode shift is by a factor of 2 larger than the experimental shift.

The linear approximation used in Fig. 6 allows a quick estimation of the *D*-mode properties. The rate at which the *D* mode shifts is proportional to the slope of the phonon dispersion and inversely proportional to the slope of the electron bands. Moreover, the excitation-energy dependence is in this approximation strictly linear.

In the next step we include, again in one dimension, the correct electronic bands from the ab initio calculation and the experimental dispersion of the TO branch. The sum over all intermediate states in Eq. (1) is performed numerically. As we showed in the last section, the main difference between the one-dimensional and the two-dimensional integration is a broadening of the range of double-resonant q values, where the positions of the maxima remain the same. Therefore, the error when performing the integration in one dimension is not larger than the uncertainties in a two-dimensional integration, where we would have to interpolate the experimental data of the phonon dispersion. Moreover, the asymmetry of the bands with respect to the *K* point (trigonal warping) is largest along the high-symmetry lines Γ–*K*–*M* and is therefore fully taken into account in the present one-dimensional calculation.

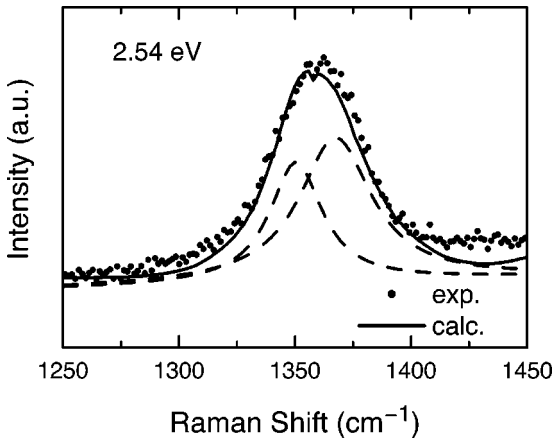

FIG. 7. Raman spectrum of the *D* mode at $E_1=2.54$ eV. The experimental spectrum (dots) was taken on a natural graphite flake. The solid line shows a spectrum calculated from the experimental data of the graphite TO phonon (Ref. 6); the dashed lines are Lorentzian fits to the calculated spectrum. The calculated Raman intensity is at each phonon energy multiplied by a Lorentzian with a full width of 20 cm^{-1}.

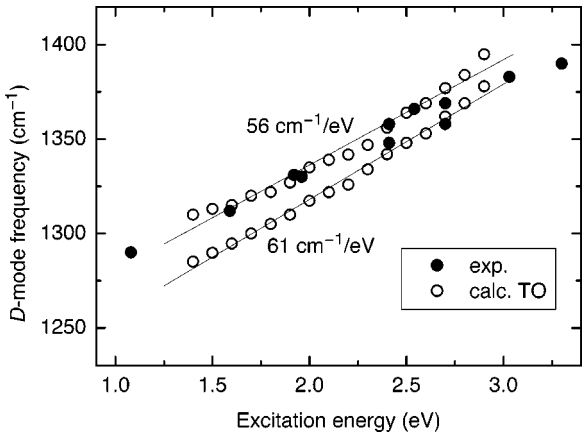

FIG. 8. *D*-mode frequency of graphite as a function of laser energy, calculated from the experimentally determined TO branch. The upper and lower frequencies come from phonons between $K-M$ and between $\Gamma-K$, respectively. The dots denote experimental data from Refs. 13, 30, and 31.

In Fig. 7, we show a calculated Raman spectrum of the *D* mode for an excitation energy $E_1=2.54$ eV. The agreement with the experimental spectrum (dots) is excellent considering that no adjustable parameter is involved except for an overall scaling. The *D*-mode peak is not a single Lorentzian but has a complex line shape due to the double-resonance processes contributing to the signal. The individual contributions are not resolved, and a fit by two Lorentzians is appropriate. Each of them roughly corresponds to phonons from one particular side of the *K* point as discussed above. The good agreement in line shape was obtained by using a phonon linewidth of 20 cm^{-1} in the calculation. This large linewidth is consistent with the broadened range of double-resonant phonon wave vectors that we expect for the integration in two dimensions.

The *D*-mode frequency as a function of excitation energy from the same calculation as in Fig. 7 is shown in Fig. 8. The frequencies were again found from a fit by two Lorentzians to the calculated spectra. The upper (lower) frequency stems from the phonon branch between *K* and *M* (Γ and *K*). The *D* mode shifts at a rate of 56 cm^{-1}/eV and 61 /cm^{-1}/eV. Because of the nonlinear electronic bands and phonon dispersion, the shift is only approximately linear. Our calculations again confirm that the *D* mode comes from the TO-derived phonon branch of graphite.[8,15,23,28] From the strong relation between graphite and carbon nanotubes we expect that this holds for carbon nanotubes as well.

V. MAPPING DISORDER-INDUCED MODES ONTO THE PHONON DISPERSION

If the Raman spectrum of a material is governed by double resonances and an excitation-energy dependence of the Raman modes can be measured, these experiments can in principle be used to find the phonon dispersion. This approach was first suggested for graphite by Saito *et al.*[18] As discussed, the procedure of finding the double-resonant phonon wave vector is rather complex, and a precise knowledge of both the electronic bands and the phonon dispersion is needed. Nevertheless, we can estimate the double-resonant phonon wave vector, neglecting the phonon energy and the details of the scattering process, by assuming $q\approx 2k_i$ for scattering across the Γ point. At a given excitation energy in the experiment, the electron wave vector k_i for a resonant transition of the incoming light is calculated from the electronic band structure. The observed Raman frequency of the double-resonant mode is then plotted at $q=2k_i$ into the phonon dispersion relation. We took the asymmetry of the bands with respect to the *K* point into account by finding k_i separately for both sides of the *K* point [corresponding to the processes (1) and (2) in Fig. 2(a)]. For double-resonant scattering across the *K* point, as shown by the dashed arrow in Fig. 5, the phonon wave vector is close to the Γ point and found approximately from the difference between $k_i(\Gamma K)$ and $k_i(KM)$. Since this procedure does not contain a full calculation of the Raman cross section, the destructive interferences have to be taken into account explicitly. Therefore, we do not include the processes in Fig. 2(b), in contrast to Refs. 18–20. Furthermore, the selection rules help to find the correct assignment of the double-resonant modes.

In Fig. 9, we show the mapping of all disorder-induced Raman peaks [Fig. 9(a)] and second-order modes [Fig. 9(b)] of graphite onto the phonon dispersion. Since any second-order overtone contains the fully symmetric representation, all overtones can contribute to the same scattering process that also leads to the *D* mode (Fig. 2). Combination modes, i.e., second-order scattering of two phonons from different branches, must in total contain a fully symmetric component. The solid lines are ab initio calculations that were shown to reproduce the experimental phonon dispersion very well.[6] The agreement of the Raman data and the calculation is good, in particular, for both optical modes and their overtones. For the acoustic modes, the assumption of zero-phonon energy is justified close to the Γ point; on the other hand, neglecting their large dispersion in the mapping proce-

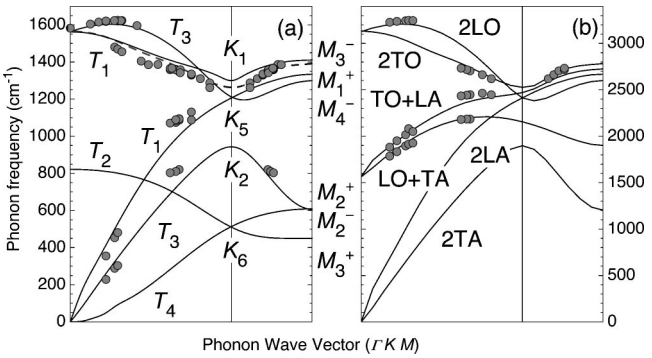

FIG. 9. (a) Disorder-induced Raman modes mapped onto the phonon dispersion of graphite (dots). Part of the experimental data are taken from Refs. 13, 30, and 32–34. The full lines are *ab initio* calculations (Ref. 6); the dashed line is a cubic-spline fit to the experimentally determined dispersion of Ref. 6. (b) Analogous mapping of the overtone and combination modes with experimental data from Refs. 32–34. The lines are the sum of the phonon branches in (a) for the overtones and the allowed combination modes.

dure leads to larger discrepancies at increasing phonon wave vectors. For more accurate results, the phonon energy should be taken into account. In contrast to Saito[18] and Kawashima,[21] we assigned the mode at $\approx$800 cm^{-1} to the transverse acoustic (TA) branch instead of the out-of-plane mode. The out-of-plane mode is forbidden by symmetry in the double-resonance process, see Sec. III, thus it cannot be seen in the Raman spectra. Furthermore, no disorder-induced peak corresponds exactly to the K point because of the interference effects discussed above.

In summary, the following procedure can be used to map the double-resonant Raman modes of graphite onto the phonon dispersion:

(i) Find along $\Gamma-K-M$, the two electron wave vectors $k_{i1,2}$ for an incoming resonance of the laser energy,

(ii) Plot the fully symmetric modes (TO, longitudinal acoustic) at $q=2k_{i1,2}$ into the phonon dispersion, and

(iii) Plot the modes with T_3 symmetry (LO, upper TA) at $q=|k_{i1}-k_{i2}|$ along $\Gamma-K-M$.

In this way, the experimental data points from Raman scattering were plotted in Fig. 9; thus, an unknown dispersion curve can be investigated experimentally with double-resonant Raman scattering.

VI. SUMMARY

In conclusion, we presented an in-depth analysis of double-resonant Raman scattering. We calculated the double-resonant D mode in graphite without using arbitrary assumptions or adjustable parameters in the calculation. We derived an analytical expression for D-mode scattering in one dimension and showed that double resonances with $q=K'$ and $q=0$ vanish by destructive interferences. The integration in the two-dimensional Brillouin zone does not alter the double-resonant phonon wave vectors found from the one-dimensional integration. We performed a full integration of the Raman cross section in one dimension, using the experimentally determined phonon dispersion of graphite. The obtained D-mode shift of 43–61 cm^{-1}/eV is in good agreement with the experiment, confirming that the D mode comes from the TO-derived phonon branch. The selection rules for double-resonant scattering along the high-symmetry directions of the graphene Brillouin zone were found and used for a mapping of disorder-induced and second-order Raman modes onto the phonon dispersion.

ACKNOWLEDGMENTS

This work was supported by the DFG under Grant No. Th 662/8-2. One of the authors (S. R.) was supported by the Oppenheimer Fund and Newnham College, Cambridge, UK.

APPENDIX

In this Appendix, we derive the expression of Eq. (2) for the Raman matrix element $K_{2f,10}$ in the case of D-mode scattering within linear bands in one dimension. From the scattering processes shown in Fig. 2(a) we find

$$E_{ai}=(|k|-K')(v_1-v_2)-i\gamma \quad \text{for } |k|<K',$$

$$E_{ai}=(-|k|+K')(v_1-v_2)-i\gamma \quad \text{for } |k|>K', \tag{A1}$$

and

$$E_{bi}=-|k|(v_1+v_2)+qv_1-K'(v_1-v_2)-i\gamma \quad \text{for } |k|<K',$$

$$E_{bi}=-|k|(v_1+v_2)+qv_2-K'(v_2-v_1)-i\gamma \quad \text{for } |k|>K', \tag{A2}$$

The double-resonant processes (1) and (2) in Fig. 2 correspond to $|k|<K'$ and $|k|>K'$, respectively. In the first case, the phonon wave vector is smaller than $2K'$, i.e., it is from between K and M, whereas in the second case q is larger than $2K'$ and stems from between K and Γ.

From the intermediate state b, the electron is scattered to a state c close to state a, therefore $E_{ci}=E_{ai}$. The phonon energy is $\hbar\omega_{\mathrm{ph}}$, thus $E_1-\hbar\omega_{\mathrm{ph}}=E_2$. We insert the above expressions into Eq. (1) and obtain

$$\begin{aligned}K_{2f,10}=&\frac{2}{(2v_1)^3}\sum_{k=0}^{K'}\left[\frac{\mathcal{M}}{(\kappa_1+K'-k)(\kappa_2+K'-k)}\right.\\&\left.\times\left(\frac{1}{(\kappa_2+K'-q/2)}+\frac{1}{(\kappa_1+K'-q/2)}\right)\right]\\&+\frac{2}{(2v_1)^3}\sum_{k=K'}^{\infty}\left[\frac{\mathcal{M}}{(\kappa_1-K'+k)(\kappa_2-K'+k)}\right.\\&\left.\times\left(\frac{1}{(\kappa_2-K'+q/2)}+\frac{1}{(\kappa_1-K'+q/2)}\right)\right].\end{aligned} \tag{A3}$$

The sum can be converted into an integral over k. A straightforward evaluation of the integral yields Eq. (2),

$$K_{2f,10} = \frac{\mathcal{M}}{2v_1^2 \hbar \omega_{\mathrm{ph}}} \left[\frac{\kappa_1 + \kappa_2 + 2K' - q}{(\kappa_1 + K' - q/2)(\kappa_2 + K' - q/2)} \ln\left(\frac{\kappa_2 + K'}{\kappa_1 + K'} \cdot \frac{\kappa_1}{\kappa_2} \right) - \frac{\kappa_1 + \kappa_2 - 2K' + q}{(\kappa_1 - K' + q/2)(\kappa_2 - K' + q/2)} \ln\left(\frac{\kappa_2}{\kappa_1} \right) \right]. \quad \text{(A4)}$$

For the scattering processes according to Fig. 2(b), an analytical expression can be derived in the same way as above:

$$\begin{aligned} K_{2f,10}^{(b)} &= \frac{2\mathcal{M}}{(2v_1)^3} \cdot \frac{1}{(\kappa_1 - \kappa_2)(2K' - q)(2\kappa_1 - 2\kappa_2 + 2K' - q)(2\kappa_2 - 2\kappa_1 + 2K' - q)} \times [(2\kappa_2 - 2\kappa_1 + 2K' - q)[-(2K' - q)\ln(-\kappa_1 \\ &\quad - K') + (2\kappa_1 - 2\kappa_2 + 2K' - q)\ln(-\kappa_2 - K') + (\kappa_1 - \kappa_2)(\ln 4 - 2\ln(-2\kappa_2 - q))] + (2\kappa_1 - 2\kappa_2 + 2K' - q)[-(2\kappa_2 - 2\kappa_1 \\ &\quad + 2K' - q)\ln(-\kappa_1 - K') + (2K' - q)\ln(-\kappa_2 - K') + (\kappa_1 - \kappa_2)(\ln 4 - 2\ln(-2\kappa_1 - q))]] \\ &= \frac{2\mathcal{M}}{(2v_1)^3} \cdot \frac{f(q, \kappa_1, \kappa_2)}{(\kappa_1 - \kappa_2)(2K' - q)[2(\kappa_1 - \kappa_2) + 2K' - q][2(\kappa_2 - \kappa_1) + 2K' - q]}. \end{aligned} \quad \text{(A5)}$$

where κ_1 and κ_2 are given by Eq. (3). The function $f(q, \kappa_1, \kappa_2)$ defined above was used in the discussion in Sec. II B. For $q_1^{(b)} = 2K'$, this expression is zero; the processes in Fig. 2(b) cancel due to destructive interference.

[1] F. Cerdeira, E. Anastassakis, W. Kauschke, and M. Cardona, Phys. Rev. Lett. **57**, 3209 (1986).
[2] F. Agulló-Rueda, E. E. Mendez, and J. M. Hong, Phys. Rev. B **38**, 12720(R) (1988).
[3] C. Thomsen and S. Reich, Phys. Rev. Lett. **85**, 5214 (2000).
[4] D. Mowbray, H. Fuchs, D. Niles, M. Cardona, C. Thomsen, and B. Friedl, in *Proc. 20th ICPS*, edited by E. Anastassakis and J. Joannopoulos (World Scientific, Singapore, 1990), p. 2017.
[5] M. L. Bansal, A. K. Sood, and M. Cardona, Solid State Commun. **78**, 579 (1991).
[6] J. Maultzsch, S. Reich, C. Thomsen, H. Requardt, and P. Ordejón, Phys. Rev. Lett. **92**, 075501 (2004).
[7] S. Reich, J. Maultzsch, C. Thomsen, and P. Ordejón, Phys. Rev. B **66**, 035412 (2002).
[8] C. Mapelli, C. Castiglioni, G. Zerbi, and K. Müllen, Phys. Rev. B **60**, 12710 (1999).
[9] J. Maultzsch, S. Reich, and C. Thomsen, Phys. Rev. B **64**, 121407(R) (2001).
[10] S. Reich, C. Thomsen, and J. Maultzsch, *Carbon Nanotubes: Basic Concepts and Physical Properties* (Wiley-VCH, Berlin, 2004).
[11] F. Tuinstra and J. L. Koenig, J. Chem. Phys. **53**, 1126 (1970).
[12] R. P. Vidano, D. B. Fischbach, L. J. Willis, and T. M. Loehr, Solid State Commun. **39**, 341 (1981).
[13] I. Pócsik, M. Hundhausen, M. Koos, and L. Ley, J. Non-Cryst. Solids **227**, 1083 (1998).
[14] C. Thomsen, Phys. Rev. B **61**, 4542 (2000).
[15] A. Ferrari and J. Robertson, Phys. Rev. B **64**, 075414 (2001).
[16] J. Kürti, V. Zólyomi, A. Grüneis, and H. Kuzmany, Phys. Rev. B **65**, 165433 (2002).
[17] P.-H. Tan, Y.-M. Deng, and Q. Zhao, Phys. Rev. B **58**, 5435 (1998).
[18] R. Saito, A. Jorio, A. G. Souza-Filho, G. Dresselhaus, M. S. Dresselhaus, and M. A. Pimenta, Phys. Rev. Lett. **88**, 027401 (2002).
[19] A. Grüneis, R. Saito, T. Kimura, L. G. Cançado, M. A. Pimenta, A. Jorio, A. G. Souza-Filho, G. Dresselhaus, and M. S. Dresselhaus, Phys. Rev. B **65**, 155405 (2002).
[20] L. G. Cançado, M. A. Pimenta, R. Saito, A. Jorio, L. O. Ladeira, A. Grueneis, A. G. Souza-Filho, G. Dresselhaus, and M. S. Dresselhaus, Phys. Rev. B **66**, 035415 (2002).
[21] Y. Kawashima and G. Katagiri, Phys. Rev. B **66**, 104109 (2002).
[22] R. M. Martin and L. M. Falicov, in *Light Scattering in Solids I: Introductory Concepts, Topics in Applied Physics vol. 8*, edited by M. Cardona (Springer, Berlin, 1983), p. 79.
[23] A. Ferrari and J. Robertson, Phys. Rev. B **61**, 14095 (2000).
[24] A. K. Sood, R. Gupta, and S. A. Asher, J. Appl. Phys. **90**, 4494 (2001).
[25] R. A. Jishi and G. Dresselhaus, Phys. Rev. B **26**, 4514 (1982).
[26] D. Sánchez-Portal, E. Artacho, J. M. Soler, A. Rubio, and P. Ordejón, Phys. Rev. B **59**, 12678 (1999).
[27] O. Dubay and G. Kresse, Phys. Rev. B **67**, 035401 (2003).
[28] C. Castiglioni, F. Negri, M. Rigolio, and G. Zerbi, J. Chem. Phys. **115**, 3769 (2001).
[29] M. Damnjanović, I. Milošević, T. Vuković, and R. Sredanović, Phys. Rev. B **60**, 2728 (1999).
[30] Y. Wang, D. C. Alsmeyer, and R. L. McCreery, Chem. Mater. **2**, 557 (1990).
[31] M. J. Matthews, M. A. Pimenta, G. Dresselhaus, M. S. Dresselhaus, and M. Endo, Phys. Rev. B **59**, R6585 (1999).
[32] Y. Kawashima and G. Katagiri, Phys. Rev. B **52**, 10053 (1995).
[33] P.-H. Tan, C. Hu, J. Dong, W. Shen, and B. Zhang, Phys. Rev. B **64**, 214301 (2001).
[34] P.-H. Tan, L. An, L. Liu, Z. Guo, R. Czerw, D. L. Carroll, P. M. Ajayan, N. Zhang, and H. Guo, Phys. Rev. B **66**, 245410 (2002).